Optics Letters

Ultrafast laser ablation of trapped gold nanoparticles

Javier Hernandez-Rueda,[1,2,*] Anne de Beurs,[1,3] and Dries van Oosten[1]

[1]Debye Institute for Nanomaterials Science and Center for Extreme Matter and Emergent Phenomena, Utrecht University, Princetonplein 5, 3584 CC Utrecht, Netherlands
[2]Kavli Institute of Nanoscience Delft, Department of Quantum Nanoscience, Delft University of Technology, Lorentzweg 1, 2628 CJ Delft, Netherlands
[3]Advanced Research Center for Nanolithography, Science Park 110, 1098 XG Amsterdam, Netherlands
*Corresponding author: fjavihr@gmail.com

Received 8 May 2019; revised 29 May 2019; accepted 30 May 2019; posted 31 May 2019 (Doc. ID 367035); published 25 June 2019

We investigate the interaction of femtosecond (fs) laser pulses with single gold nanoparticles, trapped in a linear Paul trap. We study the scattering response of the particles as a function of the polarization angle of a cw laser at three different wavelengths. These measurements provide a value of the visibility that we compare with Mie theory calculations in order to obtain an estimate of the particle radius. We monitor the particle size during ultrafast laser ablation, obtaining an accurate figure for the mass loss as a function of the fs-laser dose. We discuss the particle mass loss induced by a single fs-laser shot and its relation with the number of absorbed photons.

https://doi.org/10.1364/OL.44.003294

In many applications in research [1–5], technology [6], and healthcare [7], fast and ultrafast lasers are employed to cut, remove, and deposit material as well as to locally modify the chemical, structural, and optical properties of the target. In even more extreme examples, pulsed lasers are used to trigger nuclear fusion [8] and to generate extreme ultraviolet (EUV) light for a new generation of lithography machines [9] or, more practically, to study nerve regeneration *in vivo* after fs-laser axotomy [10]. Furthermore, in fields such as laser-based nanoparticle synthesis [11–16], EUV generation [9], and pulsed laser deposition [17,18], the interaction of light with nanoparticles is extremely relevant, as it conditions the targeted result. What all the above processes have in common is that so much energy is deposited in the target within a microscopic volume that the optical properties of the system change during an individual laser pulse due to the excitation and heating of electrons [5]. In this context, on the picosecond time scale, part of the target violently boils and actually fragments, giving rise to a distribution of particles ranging in size from single ions to micrometer-sized droplets, which subsequently fragment further. The interaction of extremely intense light and these nano- to micro-sized particles has been extensively investigated using a limited variety of geometries, i.e., aqueous solution of particles and particles deposited on substrates. These platforms combined with spectroscopic techniques and electron microscopy have shown how a strong laser excitation leads, for instance, to shape change, mass loss, permanent modifications on the plasmonic response, and ablation of the surrounding platform [2,16,19,20]. Furthermore, the dynamics of laser-excited particles has been investigated using pump and probe techniques aiding access to their ultrafast time response [21–24]. However, to understand both the dynamics and the aftermath of the process, one needs to account for the collective response of a myriad of nanoparticles (for experiments done in solution) or for the influence of the substrate, which is highly dependent on its response to the near field that surrounds the illuminated particle. Therefore, understanding the precise interaction of extremely intense light with single isolated particles, without the complications introduced by any surrounding platform, is highly relevant from both scientific and technological points of view.

In this Letter, we present a compact and optically accessible design of a Paul trap that allows us to trap single gold nanoparticles in a vacuum environment. Using the trap, we investigate the change on the optical properties of the levitating nanoparticles after femtosecond (fs)-laser pulse illumination. We measure how the scattering signal of single particles decreases as their size decreases due to the gradual mass loss via laser ablation. These subtle optical changes are characterized using polarimetry at several wavelengths. Polarimetry results are compared with calculations using Mie theory, allowing us to accurately retrieve the radius of the irradiated particle after certain laser doses. Finally, we estimate the number of atoms ejected from the particle using a single laser shot and relate it to the absorbed power.

In Fig. 1, we show a schematic of the trap system and the optical layout that surrounds it. The trap is embedded in a compact glass (BK7) vacuum chamber that is loaded using an electro-spray unit. The design is based on a quadrupole ion trap (QIT), i.e., Paul trap [25], which consists of four parallel gold-coated metallic rods with a length of 12 cm. Following the arguments in Denison [26] and Gibson *et al.* [27], the geometry of the system is chosen such that we can approximate an electric field produced with hyperbolic rods while maintaining

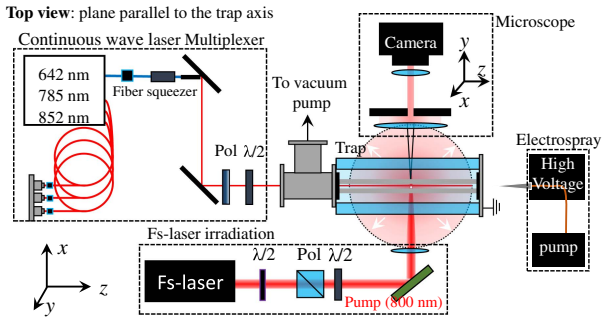

Fig. 1. Schematic of the top view of the experimental setup.

optical access. Therefore, the trap rods are arranged in a square with a side of length of $L = 8$ mm, a rod radius of $r = 3$ mm, and a rod separation of 2 mm as detailed in Fig. 2(a). We connect two diagonally opposite rods to an AC voltage while the other two are connected to a DC signal. The trap generates a time-oscillating electric quadrupole potential as denoted by formulas (1), (2) using d, r and the coordinate frame presented in Fig. 2(a). Formula 2 describes the AC signal $\phi_o(t)$ and the DC signal ϕ_1, where we set $U_{\text{seg}} = 0$ V, $V_{\text{rod}} = 600$ V and $\Omega = 6.5$ kHz using a signal generator connected to an amplifier [26,27]. Considering the geometry of the trap, the resultant time-oscillating quadrupole electric field aids to trap single gold nanoparticles that obey the Mathieu equations of motion [28]. In order to prevent the trapped particles from moving along the trap axis, we split each of the rods connected to the DC voltage into 24 electrically independent segments of 5 mm, whose voltage can be set to be either 0 V or 5 V. In this way, we generate an additional electric potential ϕ_1 that makes it possible both to fix the nanoparticles at a certain position and translate them along the z axis

$$\phi(t) = \frac{\phi_o(t)}{2(d-r)^2}(x^2 - y^2) + \phi_1, \tag{1}$$

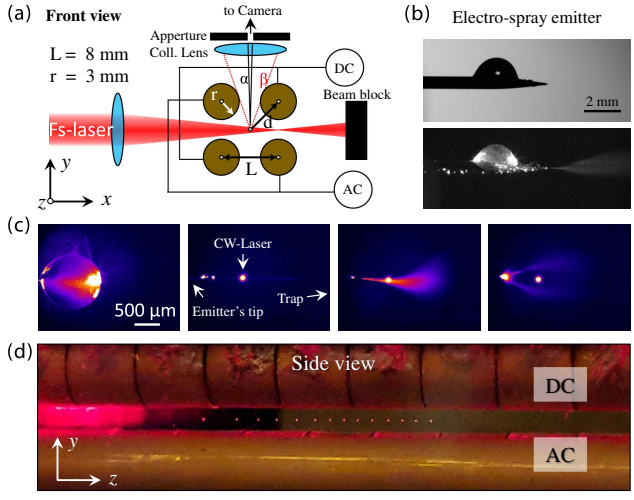

Fig. 2. (a) Schematic of the front view of the experimental setup. (b) Transmission (top) and dark field (bottom) microscopy images of the electro-spray emitter. (c) Dark field microscopy images of the electrospray cone geometries. (d) Picture of the side view of the trap with gold nanoparticles.

$$\phi_o(t) = U_{\text{seg}} + V_{\text{rod}}\cos(\Omega t), \qquad \phi_1 = 0 \text{ or } 5 \text{ V}. \tag{2}$$

The nanoparticle preparation consists of one part of an aqueous solution of gold nanospheres (nanoComposix, diameter = 100 nm, 0.05 mg/mL) mixed with nine parts of ethanol. The gold nanoparticles are introduced inside the trap by means of an electro-spray system. This unit uses a hollow fused-silica emitter with an internal diameter of 15 µm and a metallic coating (New Objective FS360-75-15) that is connected to a high voltage that ranges from 500 V to 2500 V. The emitter is attached to a 200 nm filter and a syringe that contains 10 mL of the nanoparticle solution. We use fused silica tubing with an internal diameter of 100 µm (New Objective CT360-100-25) to connect the different elements of the electro-spray unit. Figure 2(b) illustrates transmission optical microscopy and dark field microscopy images of the emitter and the electro-spray cone. The lower image presents the light scattered by the Taylor cone during the loading process. Figure 2(c) shows the different electro-spray geometries observed while optimizing the emitter voltage; the third one illustrates the one we used to load the trap. After loading the trap, we evacuate the air inside the vacuum chamber reducing the pressure to 8.1×10^{-2} mbar. Figure 2(d) shows the laser light scattered by 14 nanoparticles inside the trap.

The optical setup in Fig. 1 combines an *in situ* microscope, a cw-laser multiplexer and a fs-laser irradiation arrangement. The cw-laser system consists of a multiplexer, where we connect three pigtailed diode lasers with wavelengths of 642 nm, 785 nm, and 852 nm. We use these lasers to illuminate the trapped nanoparticles along the trap axis in order to measure their scattering response and characterize their size. To achieve linear polarization, we make use of a fiber squeezer (FS) and a polarizer (Pol), reaching 100:1 linearly polarized light. We control the polarization angle by means of a super-achromatic $\lambda/2$ wave plate and a motorized rotating mount (PI type stage). The *in situ* microscope allows us to capture the scattered light, at an angle of 90° with respect to the trap axis (z), using an electron-multiplying CCD camera (Andor, Ixon 885). The nanoparticle position was monitored at all times during the experiments using the microscope. Overall, the trap shows an excellent stability, and the nanoparticles remain at the exact same position for long periods of time (up to months). Experiments where the particle moved more than 10 pixels away from the trap axis were discarded [29]. For the irradiation experiments, we used a fs-laser regenerative amplifier that produces 150 fs-laser pulses at 800 nm and a repetition rate of 1 kHz. We used a fused-silica lens with a focal distance of 100 mm to focus the fs-laser beam on the nanoparticles, resulting in a local fluence of 0.21 J/cm^2. As shown in Fig. 2(a), we focused the beam slightly after the particle in order to obtain a larger beam size in the $y-z$ plane where the sample was trapped. By collecting the scattered signal of a nanoparticle at several positions along the z axis, we measured the beam waist ($1/e^2$) to be 50 µm.

Figure 3(a) shows an image of the light scattered by a single trapped nanoparticle that was acquired using the *in situ* microscope. In Fig. 3(b), we integrate the signal along the vertical axis of the map (black circles) and perform a Gaussian fit (red line) in order to obtain a background-free measure of the scattered signal. We experimentally observe that the fs-laser scattering signal of a single gold nanoparticle gradually decreases when we illuminate it using several consecutive laser pulses, as shown in Fig. 3(c). The total scattering cross section of a nanoparticle

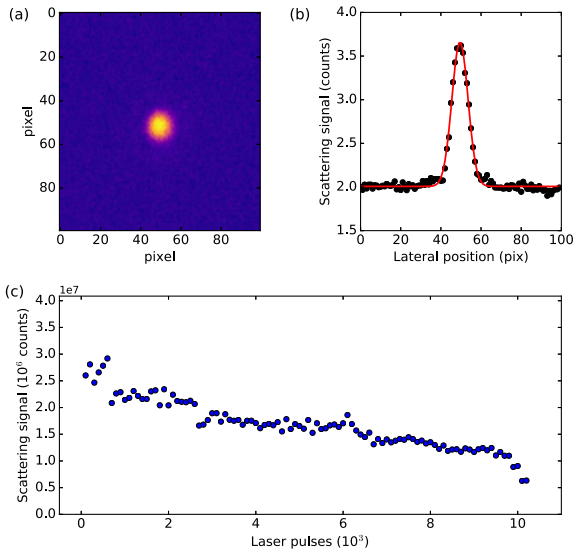

Fig. 3. (a) False color image of the scattered intensity (at 800 nm) of a single gold nanoparticle. (b) Integrated scattering intensity of the image in (a). (c) Fs-laser scattering signal of a single trapped nanoparticle as a function of the number of consecutive pulse exposures.

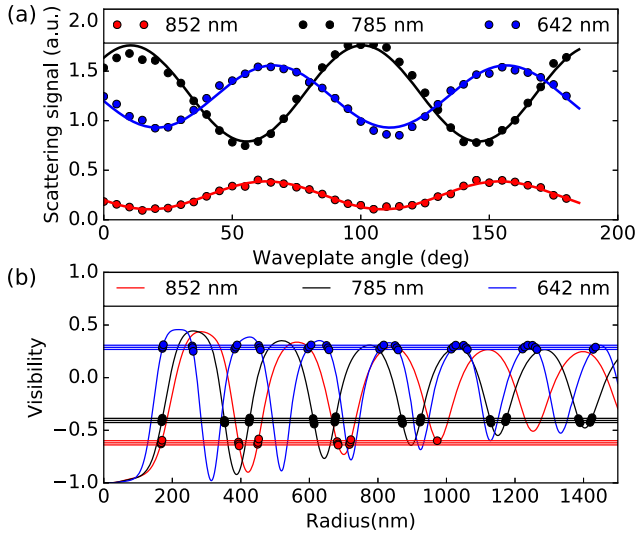

Fig. 4. (a) Graph of the polarimetry measurements performed using three different cw-laser wavelengths. The solid lines are fits using a sine function. (b) Visibility of gold nanoparticles as a function of the radius at three different wavelengths. The visibility curves were calculated using Mie theory. The horizontal lines show the experimental visibilities extracted from the fits in (a) using Eq. (4), and the circles illustrate the intersections with the Mie calculations.

at a particular wavelength depends on both its size and composition. Therefore, we attribute the observed decrease to the minute fs-laser-induced mass loss mediated by ablation, which reduces the nanoparticle size and thus its scattering cross section. To determine the laser-induced mass ejection per pulse, we estimate the size of the nanoparticles using a multi-wavelength polarimetry technique at certain stages of the ultrafast ablation experiment.

Figure 4(a) shows the polarimetry curves of a single trapped particle measured at three wavelengths, i.e., 642 nm, 785 nm, and 852 nm. The graph presents the scattering intensity as a function of the laser polarization angle when the light is collected at 90° (y axis) with respect to the incident laser direction (z axis) [see Fig. 2(a)]. Equation (3) shows the relation between the scattered (E_s) and incident (E_i) electric field through the scattering amplitude matrix, which depends on the laser frequency, the nanoparticle radius, and its dielectric function [30,31]. The subscripts indicate the perpendicular $E_\perp$ and parallel $E_\parallel$ components of the electric field with respect to the scattering plane. Equation (3) establishes that $|S_1|^2$ and $|S_2|^2$ are proportional to the intensity scattered when using a parallel or a perpendicularly polarized beam, respectively. We use the elements of the scattering amplitude matrix to define the visibility $\mathcal{V}$ in Eq. (3). Note that this definition leads to both positive and negative values and therefore contains information about what component of the electric field (i.e., $E_\perp$ or $E_\parallel$) corresponds to a maximum or a minimum of the scattered signal collected at 90° (y axis) with respect to the laser propagation direction (z axis). We then compare the experimental results with calculations of the visibility based on Mie theory to retrieve an estimate of the radius:

$$\begin{pmatrix} E_{\parallel s} \\ E_{\perp s} \end{pmatrix} = \frac{e^{ikr}}{-ikr} \begin{pmatrix} S_2 & 0 \\ 0 & S_1 \end{pmatrix} \begin{pmatrix} E_{\parallel i} \\ E_{\perp i} \end{pmatrix}, \qquad \mathcal{V} = \frac{|S_2|^2 - |S_1|^2}{|S_1|^2 + |S_2|^2}. \tag{3}$$

We use an open source Python package [32] to compute the visibility based on Mie formalism for three laser wavelengths. The solid curves in Fig. 4(b) present the calculated visibility as a function of the radius of the nanoparticle up to 1.5 μm. The visibility curves oscillate between ±1 with a period that corresponds to $\lambda/2$ and whose overall amplitude decreases as the nanoparticle size increases. The horizontal lines indicate the experimental visibility values extracted from the curves presented in Fig. 4(a) with their uncertainties. At a given wavelength, a single visibility value does not uniquely determine the radius, as illustrated by the intersections of the experimental values with the calculated curves (i.e., five possible radii at 852 nm). Therefore, we use three laser frequencies to unambiguously determine the radius. To each intersection, we assign a Gaussian probability distribution that is centered at the corresponding radius and with a width extracted from the uncertainty of the experimental visibility (see parallel horizontal lines, extracted from sine fits). Subsequently, we obtain the radius by calculating the maximum likelihood value as a result of the overlap integral of the Gaussian probability distributions for the three wavelengths, which in the present study leads to a radius of $r_o = 169.8 \pm 1.5$ nm.

Once the initial radius r_o is determined using three wavelengths, we illuminate the levitating nanoparticle using a train of fs-laser pulses. Note here that we make use of a repetition rate of 1 kHz; therefore, heat accumulation between consecutive pulses is expected to have a negligible influence [33]. If we consider the power absorbed by the particle during the exposure and assume that heat loss is due purely to thermal radiation, we can use Stefan–Boltzmann's law to find that the equilibrium temperature is at maximum 745 K. Furthermore, we estimate that this equilibrium is reached within tens of pulses, such that the equilibrium behavior dominates the effects

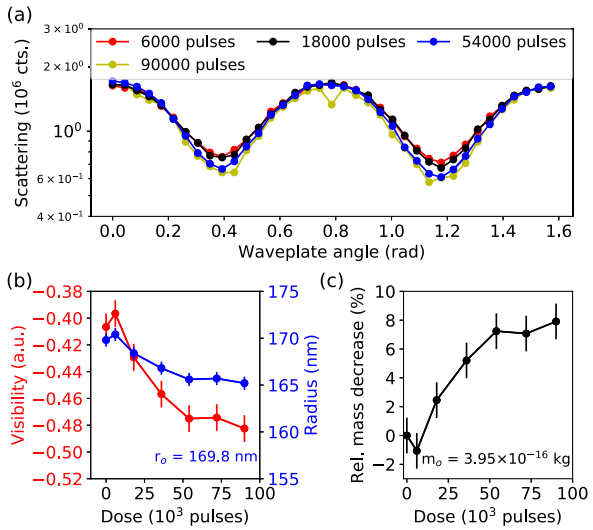

Fig. 5. (a) Experimental polarimetry curves at 785 nm of a single trapped gold nanoparticle after several fs-laser pulse exposures. This nanoparticle is the same one whose size characterization is presented in Fig. 4. Note that we set a logarithmic scale to stress the relative change of the curves. (b) Experimental visibility and radius as a function of the fs-laser dose. (c) Relative mass decrease in percentage as a function of the fs-laser pulse dose. The insets r_o and m_o indicate the radius and mass of the nanoparticle prior to laser exposure.

that we see in our measurements. We characterize the gradual size decrease of the particle by using the polarimetry method at 785 nm. Figure 5(a) shows the polarimetry curves after irradiation using 6,000, 18,000, 54,000, and 90,000 consecutive pulses. A semi-log scale is used to better illustrate the subtle change of the scattering response on the lower part of the curves. From these curves, we extract first the visibility and then the corresponding radius as a function of the dose, as shown in Fig. 5(b). The fs-laser irradiation leads to the gradual evaporation of the gold nanoparticle via ultrafast laser ablation, thus reducing its scattering cross section. We observe an overall mass decrease of an $8 \pm 1\%$ of the initial nanoparticle mass, as shown in Fig. 5(c). This leads to a total mass loss of 10^8 atoms, which corresponds to approximately 1150 atoms/pulse. The amount of photons coupled to the electrons can be calculated as $\mathcal{N} = \frac{\sigma_{\text{abs}} I}{\hbar\omega} \Delta t$, where σ_{abs} is the absorption cross section of the nanoparticle, I is the intensity of the laser, $\hbar\omega$ is the photon energy at 800 nm, and Δt is the laser pulse duration. For our experimental conditions $\sigma_{\text{abs}} = 1.46 \times 10^3$ nm^2 and $I = 1.7 \pm 0.4$ TW/cm^2, we estimate that $\mathcal{N} = 15.5 \pm 4.5 \times 10^6$ photons/pulse are absorbed, which indicates that $13.5 \pm 5.2 \times 10^3$ photons must be absorbed to eject one atom of gold.

To summarize, we have presented a quadrupole linear trap design that provides the ideal platform to study the interaction of fs-laser pulses with single nano-sized objects without the need of using a liquid environment or a glass substrate. Our combination of methods is very reliable to study the scattering response of nanoparticles during ultrafast laser ablation, bringing together two fields of photonics. We have monitored the gradual fs-laser-induced evaporation of gold nanoparticles with an extremely high accuracy, finding that 1150 atoms/pulse are ejected requiring 13.5×10^3 photons. As an outlook, we propose the combination of the current trap system with locking amplification to study the transient scattering properties of gold nanoparticles during and after fs-laser excitation.

Funding. H2020 Marie Skłodowska-Curie Actions (MSCA) (703696 ADMEP).

Acknowledgment. We thank Denise M. Krol, Peter van der Straten, Allard Mosk, Dolphine Kosters, and James Findley de Regt for fruitful discussions. We also thank Paul Jurrius, Dante Killian, Fritz Ditewig, and Cees de Kok for their technical assistance.

REFERENCES

1. S. Sundaram and E. Mazur, Nat. Mater. **1**, 217 (2002).
2. A. Plech, V. Kotaidis, M. Lorenc, and J. Boneberg, Nat. Phys. **2**, 44 (2006).
3. Y. Silberberg, Nature **414**, 494 (2001).
4. M. Vreugdenhil, D. van Oosten, and J. Hernandez-Rueda, Opt. Lett. **43**, 4899 (2018).
5. J. Hernandez-Rueda and D. van Oosten, Opt. Lett. **44**, 1856 (2019).
6. R. R. Gattass and E. Mazur, Nat. Photonics **2**, 219 (2008).
7. U. K. Tirlapur and K. König, Nature **418**, 290 (2002).
8. T. Ditmire, J. Zweiback, V. Yanovsky, T. Cowan, G. Hays, and K. Wharton, Nature **398**, 489 (1999).
9. D. Kurilovich, T. D. F. Pinto, F. Torretti, R. Schupp, J. Scheers, A. S. Stodolna, H. Gelderblom, K. S. Eikema, S. Witte, W. Ubachs, R. Hoekstra, and O. O. Versolato, Phys. Rev. Appl. **10**, 054005 (2018).
10. M. F. Yanik, H. Cinar, H. N. Cinar, A. D. Chisholm, Y. Jin, and A. Ben-Yakar, Nature **432**, 822 (2004).
11. T. E. Itina, J. Phys. Chem. C **115**, 5044 (2011).
12. M. Ullmann, S. K. Friedlander, and A. Schmidt-Ott, J. Nanopart. Res. **4**, 499 (2002).
13. S. Noël, J. Hermann, and T. Itina, Appl. Surf. Sci. **253**, 6310 (2007).
14. J. Perrière, C. Boulmer-Leborgne, R. Benzerga, and S. Tricot, J. Phys. D **40**, 7069 (2007).
15. A. V. Kabashin and M. Meunier, J. Appl. Phys. **94**, 7941 (2003).
16. J. Doster, G. Baraldi, J. Gonzalo, J. Solis, J. Hernandez-Rueda, and J. Siegel, Appl. Phys. Lett. **104**, 153106 (2014).
17. D. Geohegan, A. Puretzky, and D. Rader, Appl. Phys. Lett. **74**, 3788 (1999).
18. M. Kawakami, A. B. Hartanto, Y. Nakata, and T. Okada, Jpn. J. Appl. Phys. **42**, L33 (2003).
19. C. Langhammer, B. Kasemo, and I. Zorić, J. Chem. Phys. **126**, 194702 (2007).
20. W. Albrecht, T.-S. Deng, B. Goris, M. A. van Huis, S. Bals, and A. van Blaaderen, Nano Lett. **16**, 1818 (2016).
21. O. L. Muskens, N. Del Fatti, and F. Vallée, Nano Lett. **6**, 552 (2006).
22. H. Baida, D. Mongin, D. Christofilos, G. Bachelier, A. Crut, P. Maioli, N. Del Fatti, and F. Vallée, Phys. Rev. Lett. **107**, 057402 (2011).
23. A. A. Unal, A. Stalmashonak, G. Seifert, and H. Graener, Phys. Rev. B **79**, 115411 (2009).
24. P. V. Ruijgrok, P. Zijlstra, A. L. Tchebotareva, and M. Orrit, Nano Lett. **12**, 1063 (2012).
25. J. W. Hager, Rapid Commun. Mass Spectrom. **16**, 512 (2002).
26. D. R. Denison, J. Vac. Sci. Technol. **8**, 266 (1971).
27. J. R. Gibson and S. Taylor, Rapid Commun. Mass Spectrom. **15**, 1960 (2001).
28. W. Paul, Angew. Chem. (Int. Ed. Engl., Suppl.) **29**, 739 (1990).
29. T.-H. Chen, R. Fardel, and C. B. Arnold, Light Sci. Appl. **7**, 17181 (2018).
30. C. F. Bohren and D. R. Huffman, *Absorption and Scattering of Light by Small Particles* (Wiley, 2008).
31. Q. Fu and W. Sun, Appl. Opt. **40**, 1354 (2001).
32. J. Leinonen, http://code.google.com/p/pymiecoated/.
33. P. Zijlstra, J. W. Chon, and M. Gu, Opt. Express **15**, 12151 (2007).